Theor Appl Climatol (2012) 108:355–371
DOI 10.1007/s00704-011-0531-8

ORIGINAL PAPER

Climate change impacts on spatial patterns in drought risk in the Willamette River Basin, Oregon, USA

Il Won Jung · Heejun Chang

Received: 21 July 2011 / Accepted: 19 September 2011 / Published online: 5 October 2011

Abstract Climate change is likely to lead more frequent droughts in the Pacific Northwest (PNW) of America. Rising air temperature will reduce winter snowfall and increase earlier snowmelt, subsequently reducing summer flows. Longer crop-growing season caused by higher temperatures will lead to increases in evapotranspiration and irrigation water demand, which could exacerbate drought damage. However, the impacts of climate change on drought risk will vary over space and time. Thus, spatially explicit drought assessment can help water resource managers and planners to better cope with risk. This study seeks to identify possible drought-vulnerable regions in the Willamette River Basin of the PNW. In order to estimate drought risk in a spatially explicit way, relative Standardized Precipitation Index (rSPI) and relative Standardized Runoff Index (rSRI) were employed. Statistically downscaled climate simulations forcing two greenhouse gas emission scenarios, A1B and B1, were used to investigate the possible changes in drought frequency with 3-, 6-, 12-, and 24-month time scales. The results of rSPI and rSRI showed an increase in the short-term frequency of drought due to decreases in summer precipitation and snowmelt. However, long-term drought showed no change or a slight decreasing pattern due to increases in winter precipitation and runoff. According to the local index of spatial autocorrelation analysis, the Willamette Valley region was more vulnerable (hot spot) to drought risk than the mountainous regions of the Western Cascades and the High Cascades (cold spot). Although the hydrology of the Western Cascades and the High Cascades will be affected by climate change, these regions will remain relatively water-rich. This suggests that improving the water transfer system could be a reasonable climate adaptation option. Additionally, these results showed that the spatial patterns of drought risk change were affected by drought indices, such that appropriate drought index selection will be important in future studies of climate impacts on spatial drought risk.

I. W. Jung · H. Chang
Department of Geography, Portland State University,
Portland, OR 97201, USA

I. W. Jung · H. Chang (✉)
Institute for Sustainable Solutions, Portland State University,
Portland, OR 97201, USA
e-mail: changh@pdx.edu

1 Introduction

When water becomes scarce in a part of the water cycle, droughts result (Vidal et al. 2010). Given their cumulative nature, droughts occur over larger geographical areas and longer time spans than other natural hazards (e.g., flood, tornado, hurricane, landslide, etc.).The impacts of droughts can be assessed not only hydroclimatologically but also socioeconomically. The socioeconomic damages caused by prolonged or severe droughts are enormous. It is well-known that the dust bowl in the American mid-west in the 1930s precipitated the disruption of agriculture and major human migration to the American west (Greenough et al. 2001). In the globalized modern world, national economies are tightly linked with other nations' economies, and the damage caused by a drought in one region can affect the rest of the world. For example, a recent multi-year drought in southeastern Australia was considered as one of the leading causes of a skyrocketing rise in world's grain prices (Bond et al. 2008; Ummenhofer et al. 2009).

Spatial and temporal extent and the severity of drought risk have been quantified by multiple drought indices in the literature (Heim 2002). Meteorological droughts, caused by lack of precipitation (moisture) over a given period of time, are probably the most widely used indices in the drought literature. Many metrological drought indices have been developed, including Palmer Drought Severity Index (PDSI, Palmer 1965), the Drought Severity Index (DSI, Phillips and McGregor 1998), and the Standardized Precipitation Index (SPI, McKee et al. 1993). As an agricultural drought index, the crop moisture index was developed to measure short-term moisture conditions with regard to crop yields (Palmer 1968), which considers week-to-week crop conditions. The Standardized Runoff Index (SRI, Shukla and Wood 2008) and the Surface Water Supply Index (Dezman et al. 1982) are hydrological drought indices, which use streamflow data that represent hydrometeorological processes happening in a certain watershed. Recently, as a result of development in remote sensing techniques, a satellite-based drought index, the normalized difference vegetation index-based vegetation condition index (VCI) (Kogan 1995) was developed. VCI has been employed in several studies to detect drought onset and to measure the intensity, duration, and impact of drought in regions around the world (e.g., Quiring and Ganesh 2010; Gebrehiwot et al. 2011)

However, most drought indices often do not represent a spatial pattern of drought risk in heterogeneous hydrologic landscape regions because they are calculated using a specific location and a given period (e.g., Vicente-Serrano and Begueria 2003; Dubrovsky et al. 2005). Suppose that there are two sites having different precipitation (or runoff, soil moisture) conditions with similar intra- and inter-annual variations. Although one site may receive much more precipitation than the other arid site, the frequency of drought risk is the same. Therefore, using indices calibrated in specific locations prevents direct comparison of relative drought risk between a water-rich region and a water-poor region. Dubrovsky et al. (2005) introduced relative drought indices to allow for the comparison of spatial drought conditions. The computation of relative drought indices is the same for original drought indices. But, relative drought indices use an aggregated time series dataset from all locations instead of using data from a specific station. This concept allows us to compare relative drought risk among different regions within a large river basin.

Climate change is likely to increase the probability of drought occurrence in the sub-tropics, and low and mid-latitudes regions (Bates et al. 2008). According to the IPCC Fourth Assessment Report (IPCC 2007), multi-model ensemble results show increasing trends in extreme droughts by the end of the twenty-first century compared to the reference period of 1981–2000. This is likely to result from the acceleration of the water cycle in a warming climate (Huntington 2006). In particular, mid-latitude temperate regions with wet winters and dry summers are projected to have higher increases in prolonged dry days. This is projected to exacerbate not only water availability but also water quality and human health. To cope with drought and these associated risks, researchers and stakeholders should identify vulnerable regions, and then reduce their vulnerability by developing adaptive policies.

To date, many studies have examined climate change impacts on drought frequency and intensity using climate simulations by global climate models (GCMs). Vidal and Wade (2009) assessed future climatological drought patterns over the UK using SPI. Vergni and Todisco (2011) also used SPI to identify the potential impacts of climate change on the agricultural water balance in central Italy. Kasei et al. (2010) investigated temporal characteristics of SPI in a semi-arid region in Sahelian West Africa to provide a guide for sustainable water resource management. Lorenzo-Lacruz et al. (2010) assessed the impact of climate variation on water balance in central Spain using SPI. Kangas and Brown (2007) investigated the spatial and temporal characteristics of anomalous precipitation in the USA and characterized drought regimes using a high-resolution precipitation dataset and SPI. Strzepek et al. (2010) assessed climate change impacts on the frequency and intensity of droughts across the USA using SPI and PDSI. Krysanova et al. (2008) evaluated drought frequency in the Elbe River basin in Germany between 1951 and 2003 using SPI. Mishra and Singh (2009) also used SPI to investigate the impact of climate change on severity–area–frequency (SAF) curves for annual droughts in the Kansabati River basin, India. Additionally, using SPI, Chen et al. (2009) examined the historical trends of meteorological drought in Taiwan. However, there are few studies that addressed spatial patterns in drought risk under climate change and their associated uncertainty.

The aim of this article is to identify possible drought-vulnerable regions in the Willamette River Basin (WRB) of the PNW under climate change. We address the following research questions: (1) Will climate change affect drought frequency in the WRB, and which regions are most vulnerable to these changes?; (2) Are there any persistent spatial patterns of drought risk that are evident under different GCMs, GHG emission scenarios, and drought indices?; (3) What is responsible for the disagreement in spatial patterns of drought? To address these questions, this study employs two spatial drought indices, relative Standardized Precipitation Index (rSPI) and relative Standardized Runoff Index (rSRI). The WRB of the PNW is selected

as the study area because it is one of the regions that are most vulnerable to global warming due to the sensitivity of streamflow to snowpack (Chang and Jung 2010). For the projection of possible droughts by climate change, eight statistically downscaled climate simulations with two GHG emission scenarios, A1B and B1, are used. Additionally, this study examines spatial uncertainty in drought frequency change using spatial analysis, local index of spatial autocorrelation (LISA).

2 Hydrology of the Willamette River Basin

The hydrology of the WRB is primarily controlled by different climatic characteristics in the basin. Mean annual precipitation varies spatially, ranging from approximately 1,016 mm in the Willamette Valley to 4,440 mm in the Coast and Cascade Ranges (Laenen and Risley 1997). In addition, the intra-annual pattern of climate shows strong seasonality, characterized by wet, mild winters, and dry, warm summers; approximately 80% of precipitation falls October through May (Franczyk and Chang 2009a, b). The seasonality is one of the main causes of low flow during summer in the WRB, inducing occasional summer drought.

Geographical characteristics such as elevation and geology are also major drivers of the different hydrological regimes of the WRB (e.g., Tague et al. 2008; Chang and Jung 2010) (see Fig. 1). Chang and Jung (2010) investigated future runoff responses according to distinct elevation and geology effects. They reported that groundwater-dominated watersheds in the High Cascades could be less sensitive to climate change in terms of relative reduction in summer flow than surface-flow-dominated watersheds because deep groundwater system of the High Cascades could buffer the effects of streamflow shift due to more rainfall and earlier snowmelt during winter season. This deep groundwater system, which helps sustain summer flow, results from the region's young permeable volcanic rocks and gentle slopes (Tague et al. 2008).

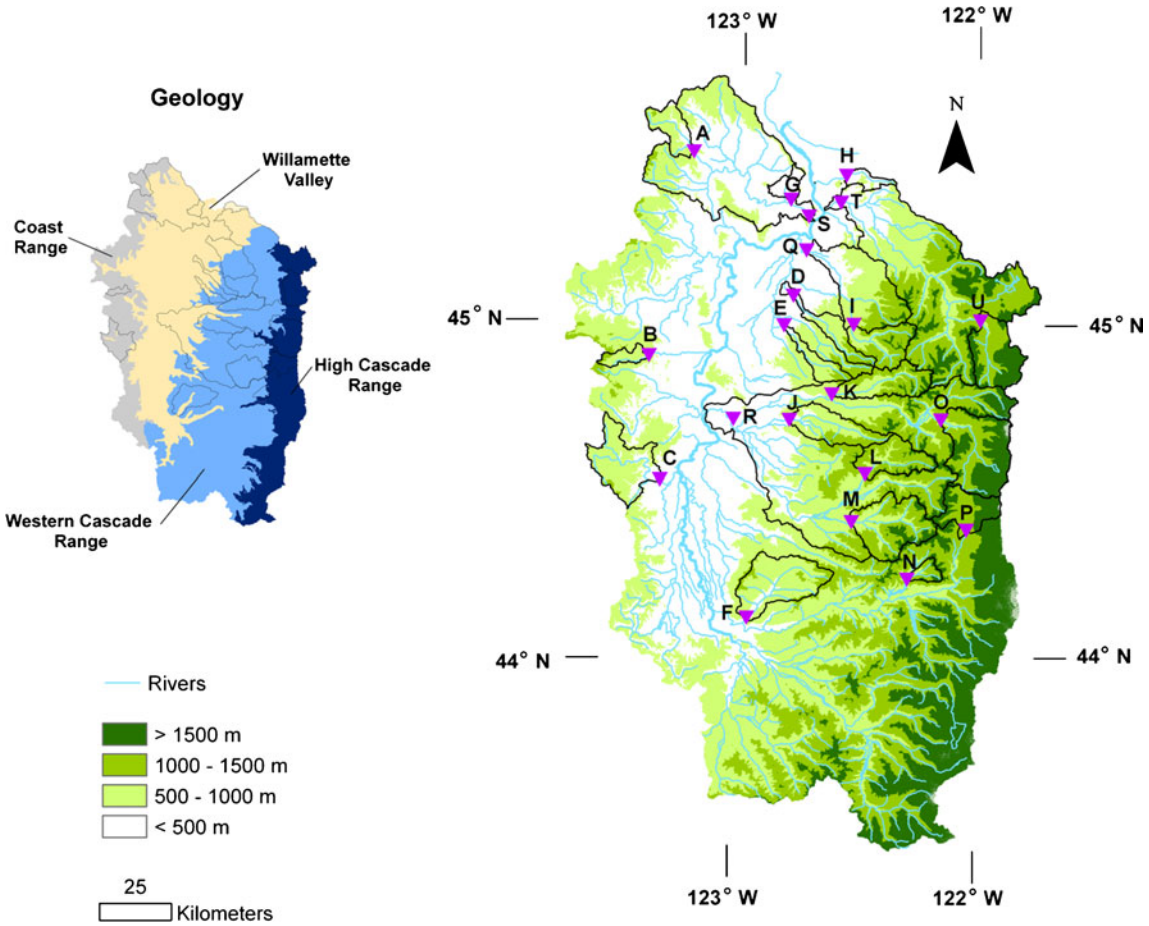

Fig. 1 The Willamette River Basin and their geology, elevation, and rivers. The *upside-down triangle* indicates streamflow gauging stations used to calibrate the PRMS model. The *black line* shows the watershed boundary

In elevations below 500 m, hydrology is highly affected by rainfall, whereas in areas above 1,500 m, river flow is dominated by snow. The snow acts as a water reservoir during winter and releases water gradually during spring and early summer. Thus, the hydrologic regime of the WRB has three distinct types: rain-dominated basins (below 500 m, 33%), transient basins (500–1,000 m, 32%), and snow-dominated basins (above 1,000 m, 35%). Given this climatic and geographic variability, it is essential to analyze potential spatial patterns in drought risk in the WRB.

3 Data and methodology

3.1 Historical and geographical data

Spatially distributed, quality-controlled hydroclimatologic datasets are required to estimate reliable drought risk. This study uses the regridded historical climate data developed by the Climate Impacts Group (CIG) at the University of Washington. The CIG used the National Climatic Data Center Cooperative Observer (COOP) network and Environment Canada (EC) station data to produce daily climate data (precipitation, maximum and minimum temperatures, and wind speed), covering the period of 1915–2006 at a spatial resolution of 0.0625° (about 7 km grid spacing). Hamlet and Lettenmaier (2005) corrected for temporal biases attributed to inhomogeneities in the COOP data by incorporating the US Historical Climatology Network and Historical Canadian Climate Database data. In addition, they considered orographic influences by employing the Precipitation Regression on Independent Slopes monthly normals (Daly et al. 1994). We used daily climate data as inputs of a hydrologic simulation model, Precipitation Runoff Modeling System (PRMS), and applied the area-averaged monthly precipitation for calculating the rSPI for each sub-basin. To calibrate the PRMS model, streamflow data were collected from the US Geological Survey National Water Information System (USGS NWIS 2011) (see Table 1). We selected 21 gauging stations that are relatively free of human impacts and complete flow records. These stations cover a wide range of elevation and geology (see Fig. 1).

Geographical datasets, including soils (NRCS 1986), land use/cover (USGS 2011), Digital elevation model with 30-m resolution (USGS 2011) and geology (McFarland 1983) are used to obtain the spatial (physical) parameters of PRMS with regard to topographic characteristics. The spatial parameters (e.g., elevation, slope, and soil type, etc.) are estimated for about 2600 Hydrologic Response Units (HRUs) that are assumed to be homogeneous with respect to their hydrologic responses to climate (Jung and Chang 2011). Based on each HRU, PRMS simulates water balance and energy balance. The spatial parameters could contribute to simulate different hydrologic regimes in the PRMS modeling.

3.2 Hydrological modeling using PRMS

PRMS is a physically based, semi-distributed hydrologic model. PRMS has been applied in the WRB to analyze the issues of water quality (Laenen and Risley 1997), water quantity (Risley et al. 2011), climate change impacts (Chang and Jung 2010), and flow trend analysis (Jung and Chang 2011). Previous studies reported that PRMS can simulate historical streamflow conditions acceptably, including snowmelt, groundwater-dominated flow (Chang and Jung 2010) as well as extreme flow (Jung et al. 2011). Chang and Jung (2010) also tested the performance of parameter regionalization of PRMS in the WRB. With regard to flow process (surface, subsurface, and groundwater flows) related parameters, the parameters of five ungauged watersheds were translated from the calibrated parameters from 12 gauged watersheds based on spatial proximity (i.e., the distance between centroids of watersheds). They categorized 218 watersheds of the WRB into four groups with different elevation and geology and translate the calibrated parameters within each group. The results showed that PRMS simulations for ungauged watersheds were acceptable in the WRB. The current study adds four new calibration sites, for a total of 16 stations. Three of the new calibration sites are located in the Western Cascades, and one is in the High Cascades. We regionalize calibrated parameters from the 16 watersheds to 5 watersheds (see Table 1) and verify the performance of PRMS.

3.3 GCM-derived climate simulations

Credible climate simulations by coupled general circulation models (GCMs) allow us to analyze changes in drought indices according to anthropogenic climate impacts. Mote and Salathé (2010) evaluated 20 GCMs from the IPCC AR4 based on how well they fit the twentieth century historical climate record in the Pacific Northwest. Because each GCM uses different atmospheric, ocean, sea ice, and land surface dynamics and resolutions, model fidelities in simulating historical climate variability and their sensitivity to greenhouse (GHG) emission scenarios vary with time and space (Randall et al. 2007). Mote and Salathé (2010) ranked GCMs based on performances of the twentieth century climate bias, a global performance index, and North Pacific variability of temperature, precipitation, and sea level pressures. CIG examined climate change impact on the hydrology of Columbia River Basin based on the analysis by Mote and Salathé (2010). This study employs eight GCM

Table 1 PRMS model performance of monthly streamflow simulations for calibration and verification periods

Elevation and geology	Watersheds for calibration					Watersheds for regionalization				
	Name(elev, m)	Cal Ver	NSE	Log-NSE	*d*	Name (elev,m)	Cal Ver	NSE	Log-NSE	*d*
Low and Coastal valley	[A]Gales Creek (707)	73–77	0.95	0.92	0.99	[Q]Molalla River (676)	00–06	0.91	0.81	0.98
		78–81	0.96	0.91	0.99					
	[B]Rickreall Creek (795)	73–76	0.95	0.87	0.99	[R]Santiam River (920)	73–06	0.84	0.75	0.96
		77–78	0.95	0.86	0.99					
	[C]Marys River (584)	73–77	0.97	0.80	0.99					
		78–85	0.94	0.81	0.98					
	[D]Butte Creek (787)	73–77	0.96	0.94	0.99					
		78–85	0.94	0.91	0.98					
	[E]Silver Creek (830)	73–77	0.97	0.90	0.99					
		78–79	0.87	0.88	0.97					
	[F]Mohawk River (752)	73–82	0.94	0.80	0.99					
		83–97	0.93	0.88	0.98					
Low and Coastal valley and urban	[G]Fanno Creek (410)	01–04	0.90	0.88	0.98	[S]Tualatin River (501)	73–06	0.93	0.88	0.98
		05–06	0.84	0.87	0.96					
	[H]Johnson Creek (470)	88–98	0.95	0.93	0.99					
		99–06	0.92	0.82	0.98					
Medimum and Western Cascade	[I]Molalla River (1,167)	73–82	0.93	0.89	0.96	[T]Clackamas River (1,138)	73–83	0.91	0.83	0.98
		83–93	0.92	0.92	0.98					
	[J]Thomas Creek (871)	73–80	0.94	0.92	0.98					
		81–87	0.94	0.91	0.99					
	[K]Lookout Creek (1,300)	73–82	0.91	0.91	0.98					
		83–97	0.91	0.92	0.97					
	[L]Little North Santiam River (1,126)	73–83	0.88	0.90	0.96					
		84–06	0.90	0.89	0.97					
	[M]Quartzville Creek (1,227)	73–83	0.90	0.91	0.97					
		84–06	0.92	0.91	0.98					
	[N]South Santiam River (1,206)	73–83	0.92	0.88	0.98					
		84–06	0.92	0.85	0.98					
High and High Cascade	[O]Mckenzie River at Clear Lake (1,565)	80–90	0.76	0.80	0.92	[U]Big Bottom (1,484)	50–68	0.71	0.75	0.91
		91–06	0.76	0.80	0.92					
	[P]North Santiam River BLW (1,569)	73–83	0.82	0.85	0.95					
		84–06	0.83	0.85	0.95					

r Correlation coefficient, *d* index of agreement, *NSE* Nash–Sutcliffe efficiency coefficient

Nash–Sutcliffe efficiency (NSE) $= \left[\sum (O_i - \overline{O})^2 - \sum (O_i - S_i)^2\right] / \sum (O_i - \overline{O})^2$, where O is observed flow and s is simulated flow and $\overline{o}$ is mean observed flow

Index of agreement (d) $= 1 - \left[\sum (S_i - O_i)^2 / \left(\sum \left(|S_i - \overline{O}| + |O_i - \overline{O}|\right)^2\right)\right]$

Letter symbols indicate the locations of streamflow gauging stations (Figure 1) used for calibration of PRMS parameters

simulations—CCSM3, CNRM-CM3, ECHAM5/MPI-OM, ECHO-G, IPSL-CM4, MIROC3.2 (hires), PCM, and UKMO-HadCM3. The biases of these GCM simulations were corrected using the bias-correction and spatial disaggregation method (Wood et al. 2004). To consider the effect of GHG emission scenarios, A1B and B1 scenarios were used. More details can be found in Salathé et al. (2007).

3.4 Sensitivity analysis by climate change and drought indices

Distinct regimes of hydrology attributed to different geology and elevation could cause different responses to climate change (Chang and Jung 2010). These different responses might affect changes in the spatial patterns of drought risk of the WRB. Additionally, different drought indices such as SPI, SRI, rSPI, and rSRI could influence drought risk analysis. We examine climate sensitivity of two representative watersheds, the Little North Santiam River near Mehama (LNR) (the L in Table 1) and the North Santiam River below Boulder Creek (NSR) (the P in Table 1). The LNR is located in Western Cascade (1,126 m), whereas the NSR is within the High Cascades (1,569 m). They have similar precipitation but different streamflow regimes because of different elevation and geology effects (see Fig. 1). The streamflow of the LNR shows high monthly variation (low summer flow), but the NSR has less fluctuation (high summer flow) due to the deep groundwater system of the High Cascades. We also analyzed drought risk by different drought indices in both watersheds.

3.5 Relative SPI and SRI

For the computation of rSPI and rSRI indices, precipitation and runoff data must be transformed into a standardized normal distribution using Eq. 1. However, precipitation and runoff data are generally positively skewed and do not fit normal (Gaussian) distribution, so these data should be adjusted to appropriate probability distribution (e.g., the Gamma, log-Normal, and Pearson Type III distributions) before normalization using the inverse Gaussian function (Ψ^{-1}) (McKee et al. 1993). This study adopts the Gamma distribution as theoretical probability distribution of precipitation and runoff. Guttman (1999) compared five distributions and reported that the Pearson Type III distribution and Gamma distribution can give robust and reliable results. Additionally, the Gamma distribution has been widely employed for calculating the

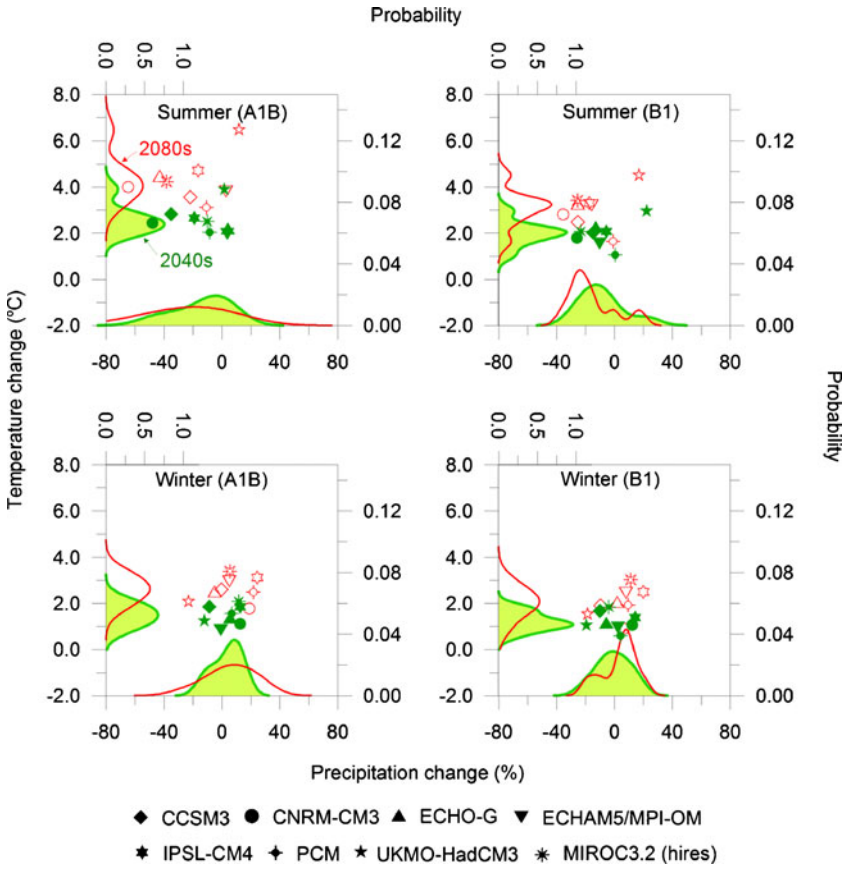

Fig. 2 Changes in seasonal precipitation and temperature according to GCMs and GHG emission scenarios over the Willamette River Basin. Probability density function is calculated using the Parzen window with Gaussian kernel estimator (Parzen, 1962)

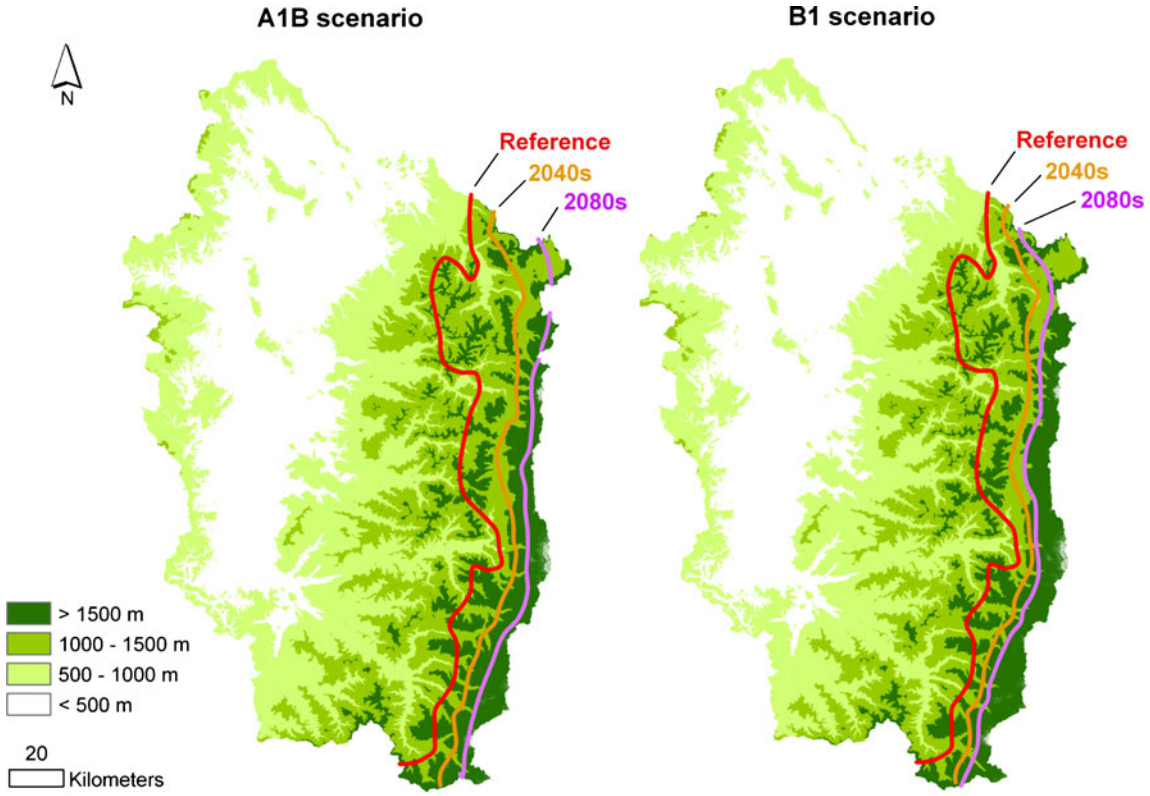

Fig. 3 December freezing levels for the reference, the 2040s and the 2080s periods. The freezing level is defined by the 0°C contour line of the mean December temperature. Each freezing level is calculated using averaging temperature of eight GCM's simulations

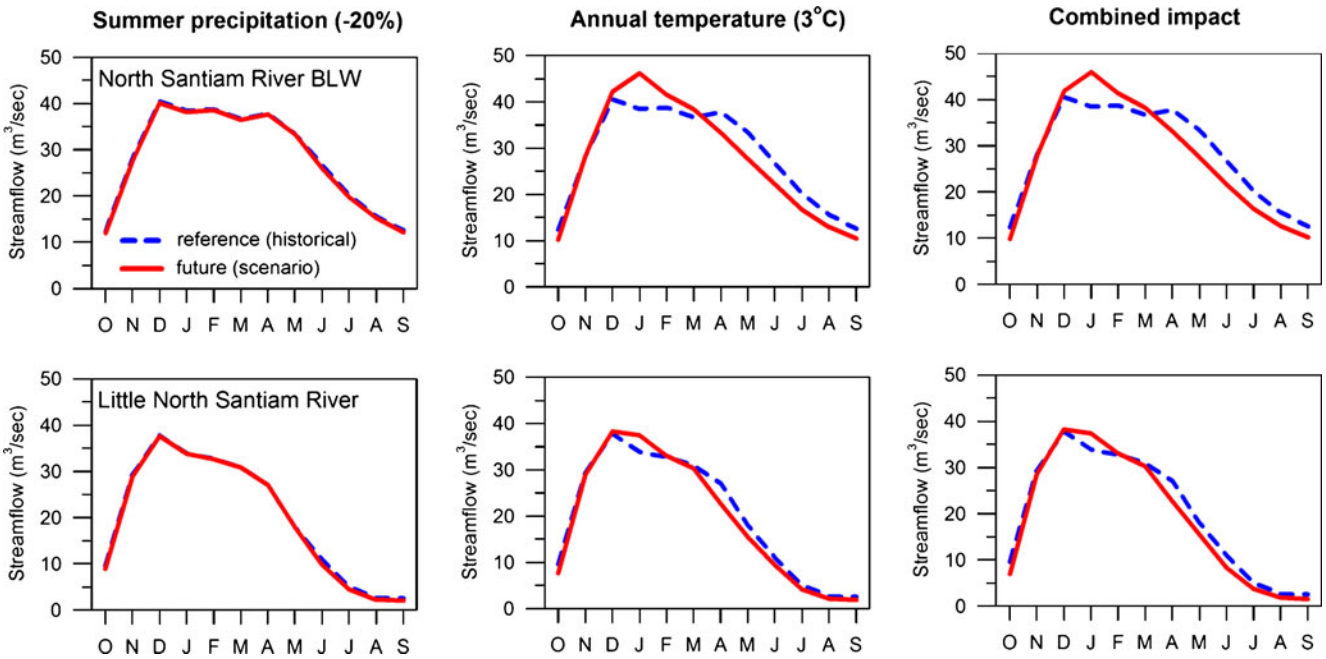

Fig. 4 The monthly flow of the North Santiam River (*upper panel*) and the Little North Santiam River (*lower panel*) according to different climate conditions such as decrease in summer precipitation (−20%), increase in temperature (3°C), and combined conditions (−20%) summer precipitation decrease and +3°C temperature increase. The climate and streamflow data used in the reference and the future periods are based on historical data for 1961–2005

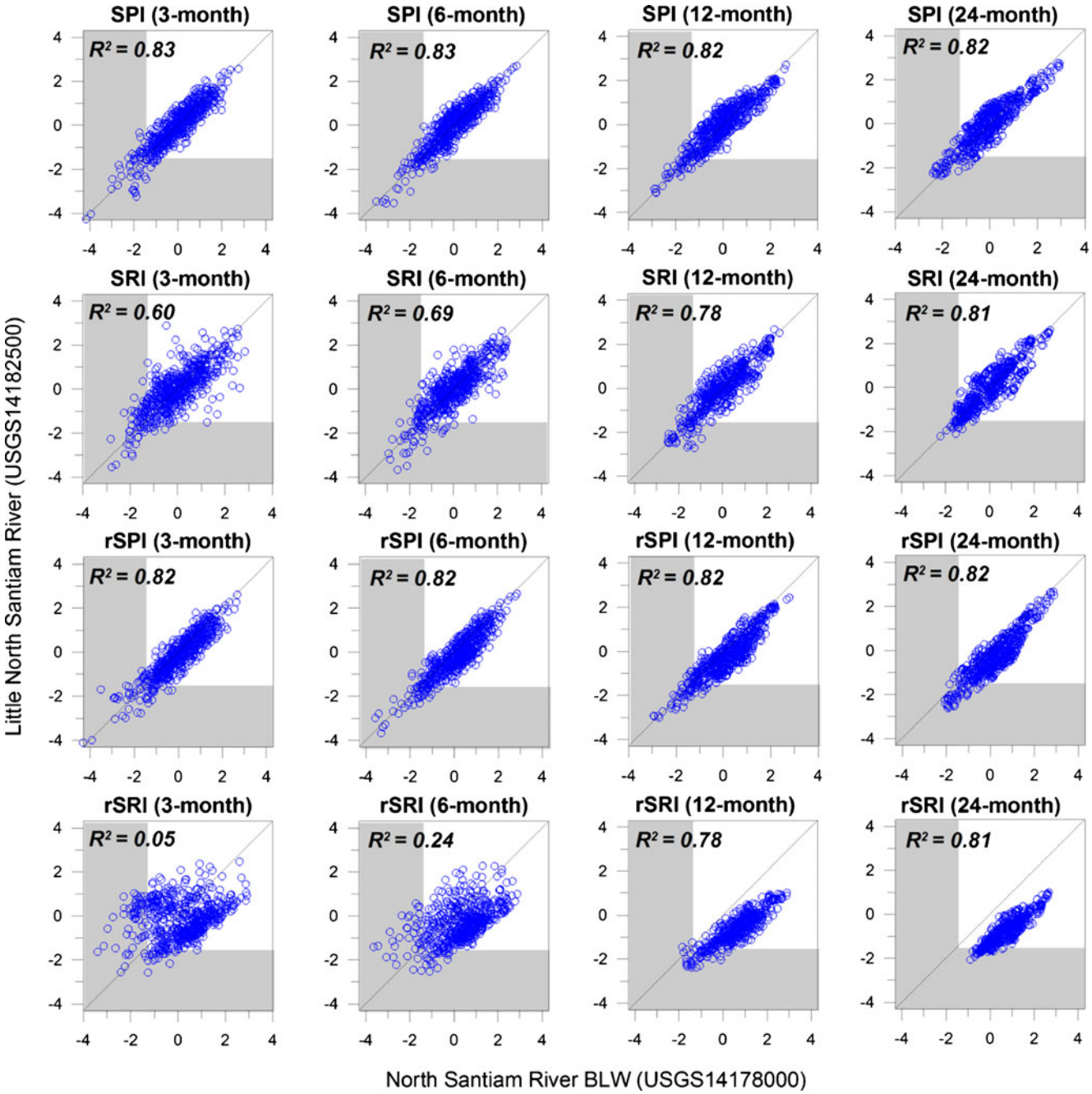

Fig. 5 SPI and SRI (*upper two panels*) and rSPI and rSRI (*lower two panels*) of Little North Santiam River at the Western Cascade (*x*-axis, the L in Fig. 1) and of North Santiam River below the Boulder Creek at the High Cascade (*y*-axis, the P in Fig. 1) using observed precipitation and streamflow for 1961–2005

SPI (e.g., Dubrovsky et al. 2009; Vidal and Wade 2009) and SRI (e.g., Shukla and Wood 2008).

$$\text{rSPI (or rSRI)} = \frac{x - x}{\sigma} = \Psi^{-1}(G(x)) \quad (1)$$

This study considers four time scales: 3, 6, 12, and 24 months. Short-term droughts (e.g., 3 and 6 months) may relate to agricultural drought that occurs at a critical time during the growing season. Long-term droughts (e.g., 12 and 24 months) may represent hydrological droughts because long-term water deficits induce severe water supply problems, reducing streamflow, groundwater, and reservoir storage. To calculate input data for each time scale, monthly precipitation and runoff data were summed using a moving window. These cumulative data points were then fitted to cumulative gamma distribution ($G(x)$) using

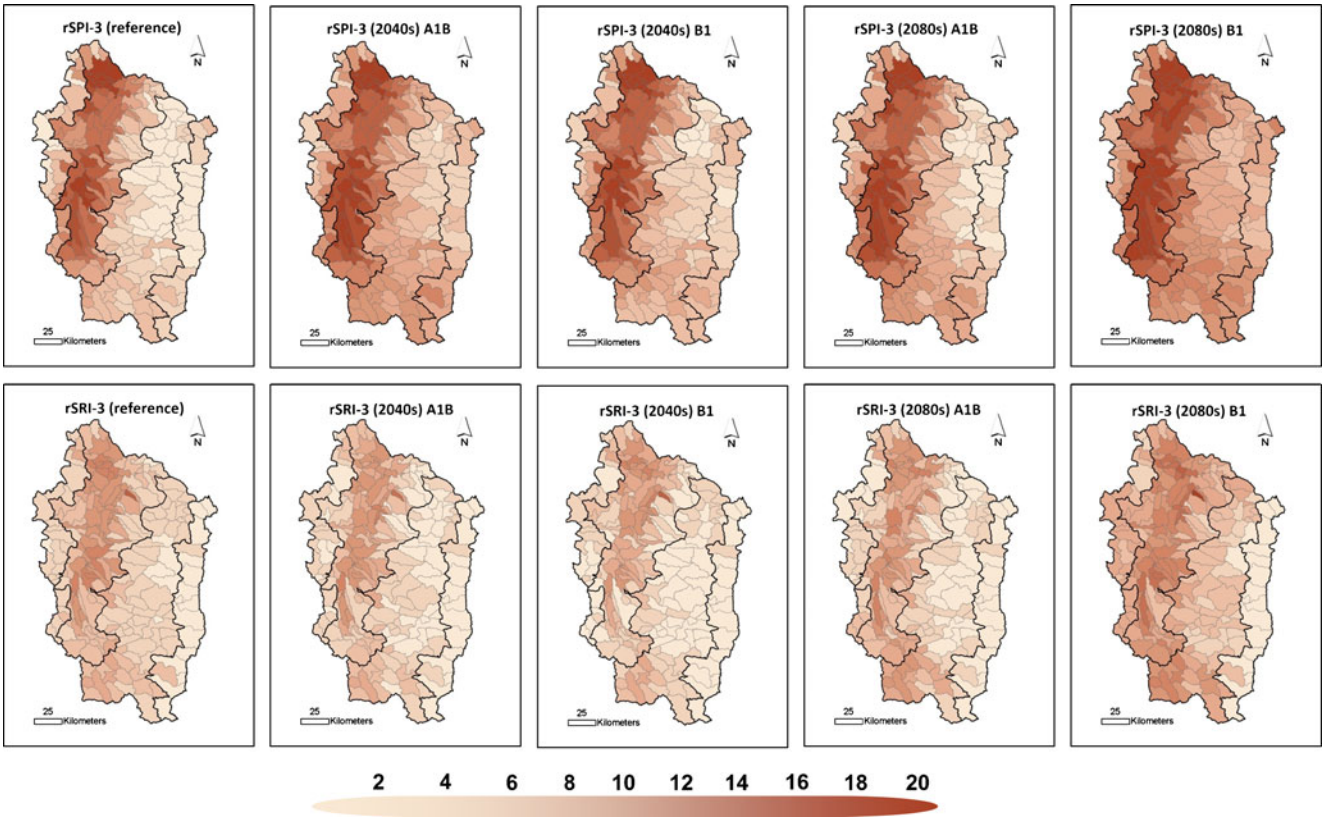

Fig. 6 Frequency of 3-month drought of rSPI (*upper panels*) and rSRI (*lower panels*) for reference, the 2040s, and the 2050s with A1B and B1 GHG emission scenarios

Eq. 2. This study uses the maximum probability solutions to determine α and β (Eqs. 3–5) (McKee et al. 1993; Guttman 1999). Each fitted distribution was then equiprobably transformed to the standard normal distribution using Eq. 1.

$$G(x) = \frac{1}{\beta^{\alpha}\Gamma(\alpha)} \int_0^x \mathrm{x}^{\alpha-1}\mathrm{e}^{-\mathrm{x}/\beta}\mathrm{dx} \tag{2}$$

$$U = 1n(\overline{\mathrm{x}}) - \frac{\sum 1n(x)}{n} \tag{3}$$

$$\alpha = \frac{1}{4U}\left(1 + \sqrt{1 + \frac{4U}{3}}\right) \tag{4}$$

$$\beta = \frac{\overline{\mathrm{x}}}{\alpha} \tag{5}$$

where α is the shape parameter of the Gamma distribution, β is the scale parameter. x is the precipitation (or runoff) of the cumulative time series and x is the mean value. $\Gamma(\alpha)$ is the Gamma function.

This procedure is first applied to aggregated data from a set of 218 watersheds of WRB for 1960–1989 as a reference period. The characteristics of the rSPI and rSRI time series in the reference period are applied to the two future periods—2040s (2030–2059) and 2080s (2070–2099)—to estimate changes in drought frequency. McKee et al. (1993) classified drought severity by SPI value: mild (0 to −0.99), moderate (−1 to −1.49), severe (−1.5 to −1.99), and extreme (−2 or less). This study focuses on investigating changes in the severe drought frequency (below −1.5).

3.6 Spatial analysis

Spatial analysis of drought risk due to climate change can identify the more vulnerable regions. However, the particular location and extent of the vulnerability can vary according to GCM simulations, GHG emission scenarios, or drought indices. To examine whether the spatial patterns of drought risk change is persistent across different GCMs, GHG emission scenarios, and drought indices, this study employs LISA (Anselin 1995). LISA can estimate spatial dependence or autocorrelation that is defined as the coincidence of value similarity with locational similarity. Thus, there is positive local autocorrelation when high/low values of drought frequency changes tend to cluster in

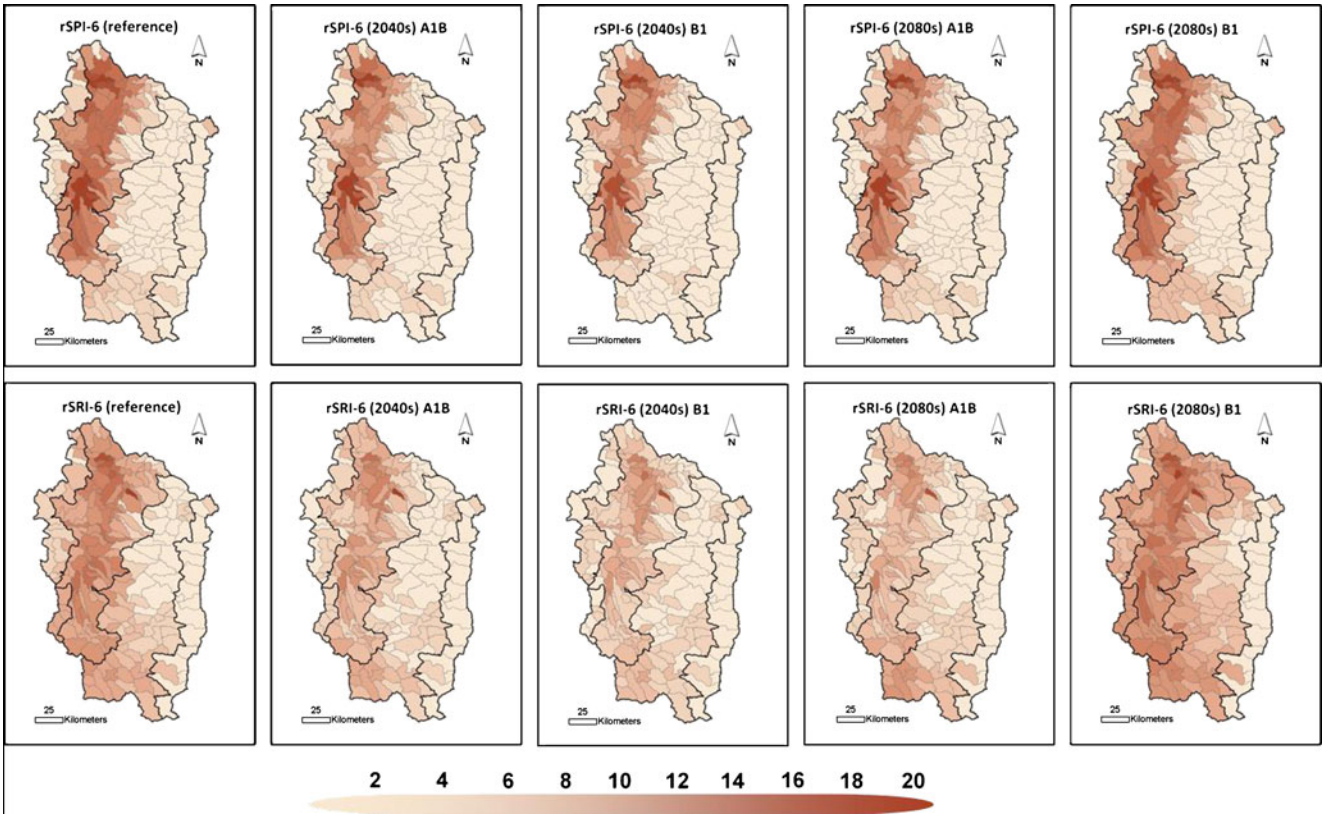

Fig. 7 Frequency of 6-month drought of rSPI (*upper panels*) and rSRI (*lower panels*) for the reference, the 2040s, and the 2050s with A1B and B1 GHG emission scenarios

space (hot/cold spots), and there is negative local autocorrelation when watersheds tend to be surrounded by neighbors with very dissimilar drought frequency changes (Anselin 1995). Therefore, if the locations of hot spot according to GCM simulations (or GHG emission scenarios, drought indices) are different, the drought analysis would be affected by GCM simulations as one of main uncertainty sources. The spatial analysis software, GeoDa (Anselin et al. 2006) is employed to determine the degree of spatial interdependence among 218 watersheds based on their drought frequency changes. This study tests the significance of LISA using a randomized test with 999 permutations and at a significance level of $p<0.01$.

4 Results

4.1 Hydrologic model calibration

To calculate rSRI, a credible hydrologic simulation is essential. We investigated how well PRMS simulations fit the observed flow using three statistical indices, Nash-Sutcliffe efficiency (NSE), log NSE, and index of agreement (d) (Willmott 1982). An NSE value of 1 indicates a perfect fit. A negative value of NSE means that the average observed flow is a better predictor than the simulated values of the hydrological model. The NSE values of daily simulated streamflow in the 16 watersheds (A to P in Table 1) show acceptable ranges, between 0.62 and 0.93 for the calibration period and between 0.58 and 0.90 for the verification period (not shown). The NSE sometimes overestimates model performance during high flow conditions and underestimates during low flow conditions (Krause et al. 2005). As an alternative, the log NSE was employed to reduce the sensitivities to such extreme values. The log NSE values are similar to the values of NSE in this study. The Willmott's index of agreement (d) is over 0.88 for the calibration and over 0.86 for the verification period, indicating a strong positive correlation. Because monthly flow was used to calculate rSRI, we also examined the monthly performance of PRMS (see Table 1). The NSE and log NSE values of monthly flow are higher than 0.76 at Clear Lake (O in Table 1), indicating a very close fit to observed monthly flow. The Willmott's index of agreement also shows acceptable ranges above 0.92 for all watersheds for both calibration and verification periods.

We examined the performance of PRMS for regionalized watersheds, whose PRMS parameters were obtained from the calibrated parameters of 16 neighboring watersheds. The PRMS performance for five regionalized watersheds

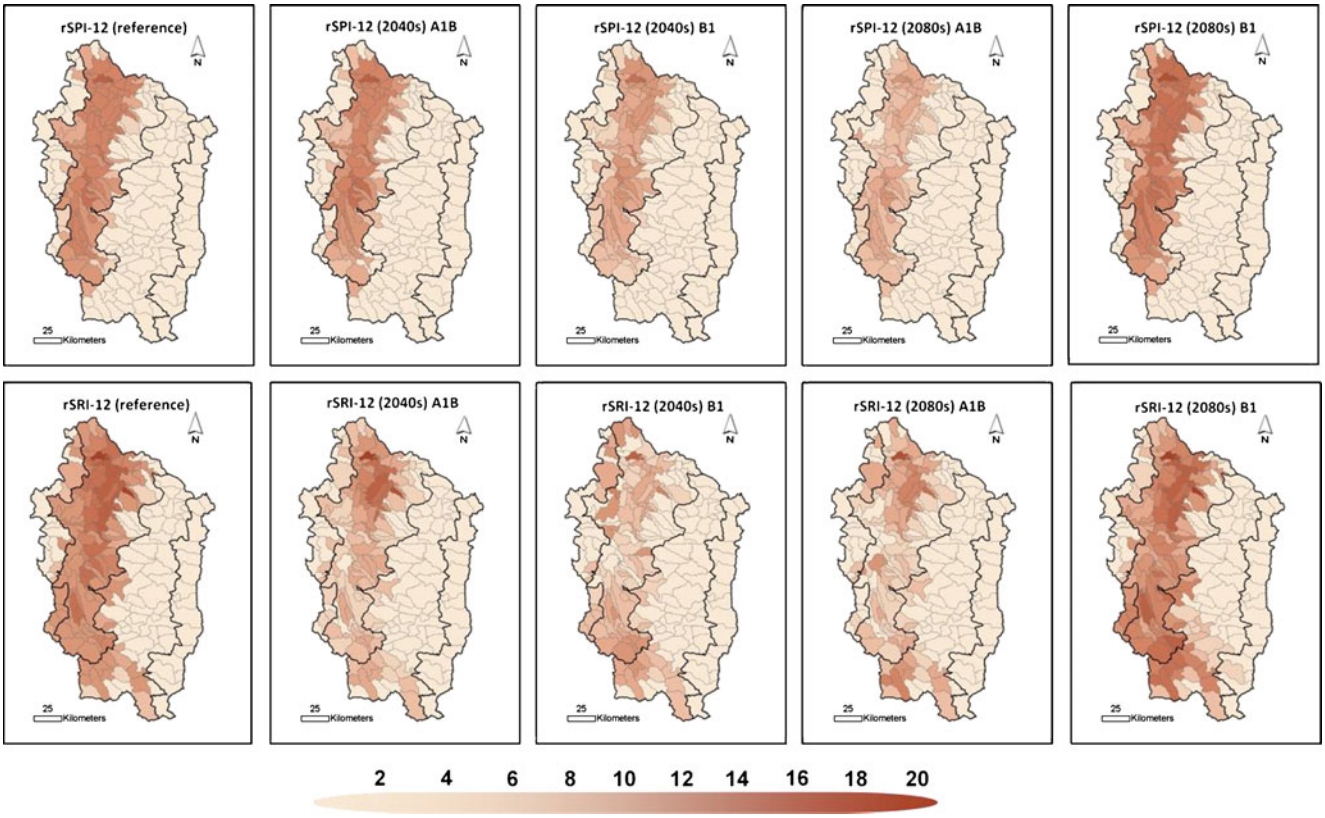

Fig. 8 Frequency of 12-month drought of rSPI (*upper panels*) and rSRI (*lower panels*) for the reference, the 2040s, and the 2050s with A1B and B1 GHG emission scenarios

shows acceptable range of statistical indices (see right of Table 1). Thus, the PRMS model used in this study shows acceptable performance for simulating different hydrologic regimes of the WRB.

4.2 Future change in climate and freezing levels

Figure 2 shows change in seasonal precipitation and temperature of WRB and their associated probability estimated by Gaussian Kernel estimator. Although the precipitation and temperature changes were highly affected by each GCM and GHG emission scenario, there were some consistent changes such as temperature increase and summer precipitation decrease. Winter temperature increases have potentially major impacts on the snowfall and snowpack in the upland of WRB that is first sensitive to global warming effect. Figure 3 shows that the elevation of freezing levels in December increases through time, indicating reduced snowpack. The combined effect of reduced snowpack and decreased summer precipitation in the WRB will decrease the summer water supply. This summer supply is essential for irrigation, residential and commercial water use during dry season (growing season), and these reductions will lead to more frequent summer droughts.

4.3 Sensitivity analysis by climate change and drought indices

Based on the projections of GCMs, we consider three possible scenarios for climate sensitivity analysis: 20% decreases in summer (June, July, and August) precipitation, 3°C increase in annual temperature, and a combination of both scenarios. Figure 4 shows the different hydrologic responses to these three climate change scenarios. The NSR and LNR are both sensitive to temperature change, but are less affected by summer precipitation decreases because the amount of summer precipitation is relatively small compared to other seasons. The NSR's streamflow changes due to temperature increases are greater than those of the LNR. However, the NSR still shows higher summer flows than the LNR, indicating that the NSR will remain a water-rich region despite significant climate change impact. Thus, the relative water availability should be considered in spatial drought risk analysis.

Figure 5 shows the comparison between drought indices of both watersheds with distinct hydrologic regimes, the LNR and NSR. The results show that SPI is similar between the two watersheds regardless of the time scales whereas SRI is quite different, especially in short-term drought (see Fig. 5). One of the reasons is that SRI can consider seasonal shift due to

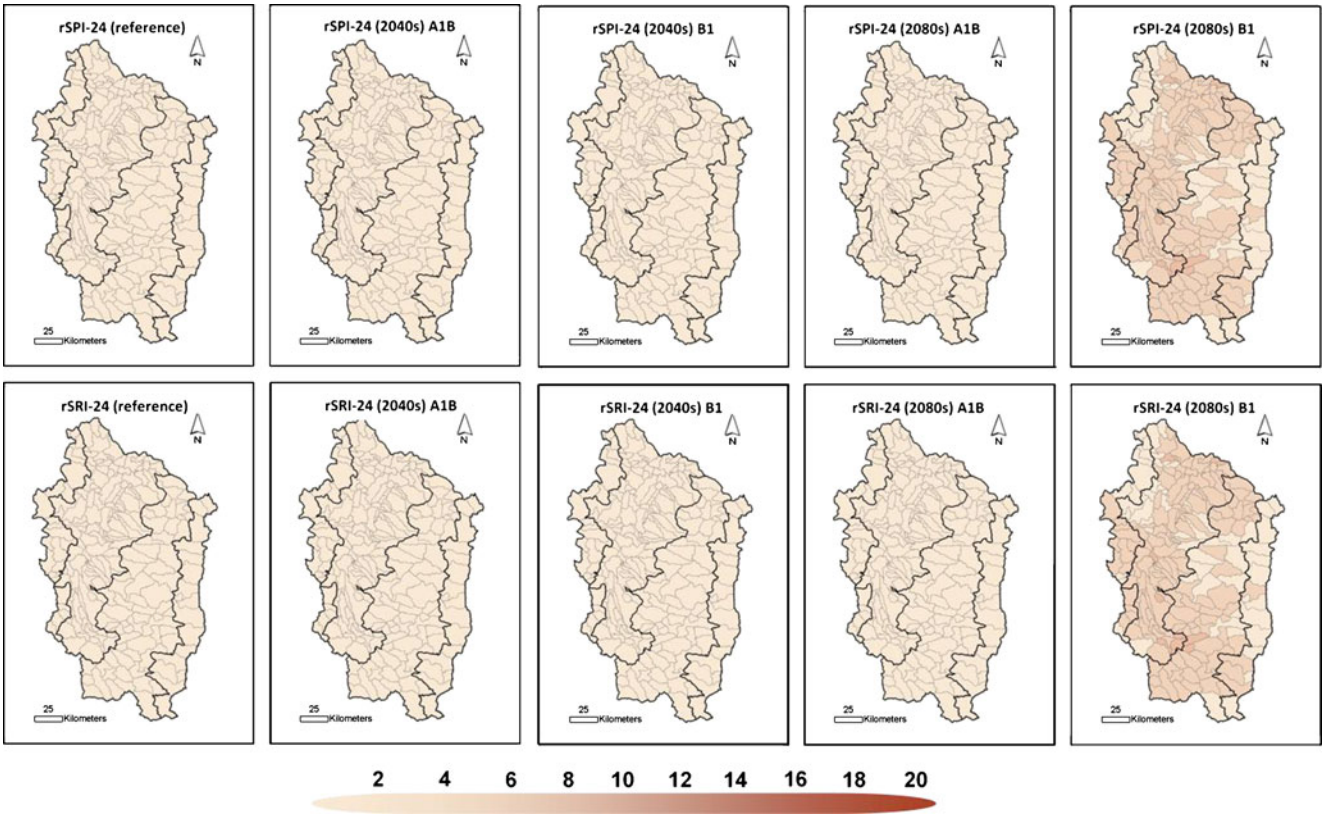

Fig. 9 Frequency of 24-month drought of rSPI (*upper panels*) and rSRI (*lower panels*) for the reference, the 2040s, and the 2050s with A1B and B1 GHG emission scenarios

snowmelt and deep groundwater system but SPI cannot represent seasonal lags of water. Shukla and Wood (2008) suggested that SRI is a useful index to examine drought risk with monthly or seasonal time scales. However, long-term SPI and SRI between the two watersheds gave similar results because of high correlation between precipitation and streamflow. The high correlation could be attributed to the removal of the seasonal lag of streamflow. This indicates that SPI is a useful short-term drought index in rainfall-dominated regions such as the Willamette Valley. However, SRI can depict more realistic short-term drought risk changes in snow-dominated regions such as the Western Cascades and the High Cascades. For relative drought analysis, rSPI shows similar results in both watersheds because their precipitation amounts are similar. Hence, short-term rSRI shows quite different values between the two watersheds. This might be due to different lag times of streamflow. As shown in Fig. 5, the rSPI and rSRI of NSR have higher values than those of LNR because the amount of precipitation and runoff of NSR are bigger than LNR. This shift can indicate relative water availability.

4.4 Spatial drought risk analysis

Figures 6, 7, 8, and 9 show the spatial patterns of changes in extreme drought frequency by rSPI and rSRI based on multi-model ensemble results under A1B and B1 GHG emission scenarios. Both drought indices indicate that the Willamette Valley is more vulnerable to drought risk than other regions for all drought time scales. This may be because the Willamette Valley has lower absolute precipitation shallower aquifer systems, and less water holding capacity and recharge than the Western Cascades and High Cascades regions. The rSPI shows increasing frequency of short-term drought over the whole Willamette River basin due to summer precipitation decrease, especially under the B1 GHG emission scenario (see Fig. 2). However, 3-month rSRI in the High Cascades depicts no change of drought frequency because the High Cascades have a deep groundwater system as discussed in Section 4.3 (see Fig. 6). Six-month rSPI does not show significant changes. However, rSRI shows increase in the frequency of drought risk in the Western Cascades region under the B1 scenario at the 2080s period (see Fig. 7). This could be attributed to the combined impact of snowmelt decrease during spring season and precipitation decrease during summer season (see Figs. 2 and 3). Long-term extreme droughts do not increase significantly with either drought index. Under the A1B scenario, 12-month rSPI and rSRI decrease because winter precipitation and streamflow increases, resulting in increasing annual values (see Fig. 8). In addition, a

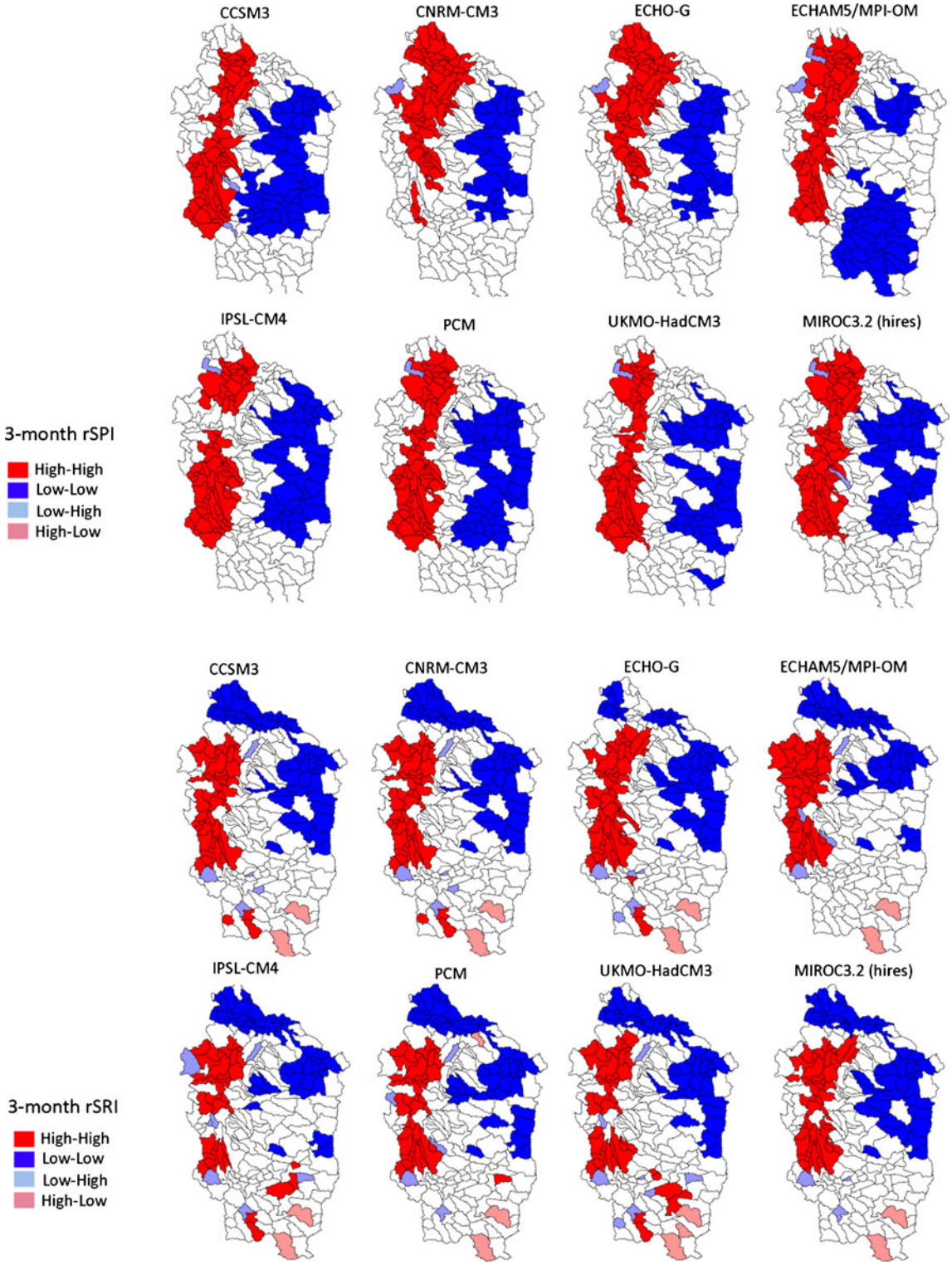

Fig. 10 Results of LISA for 3-month rSPI (*upper two panels*) and rSRI (*lower two panels*) according to eight GCMs with A1B GHG emission scenario. High–High is hot spot and Low–Low is cold spot. This analysis is based on the result of the 2080s period

decrease in 24-month droughts is predicted under most scenarios, except in the 2080s period under the B1 scenario (see Fig. 9). This is also because of increasing winter precipitation and streamflow.

4.5 Uncertainty in spatial drought analysis

As mentioned in Section 4.4, the 3-month extreme drought frequency increases in future time slices. This study

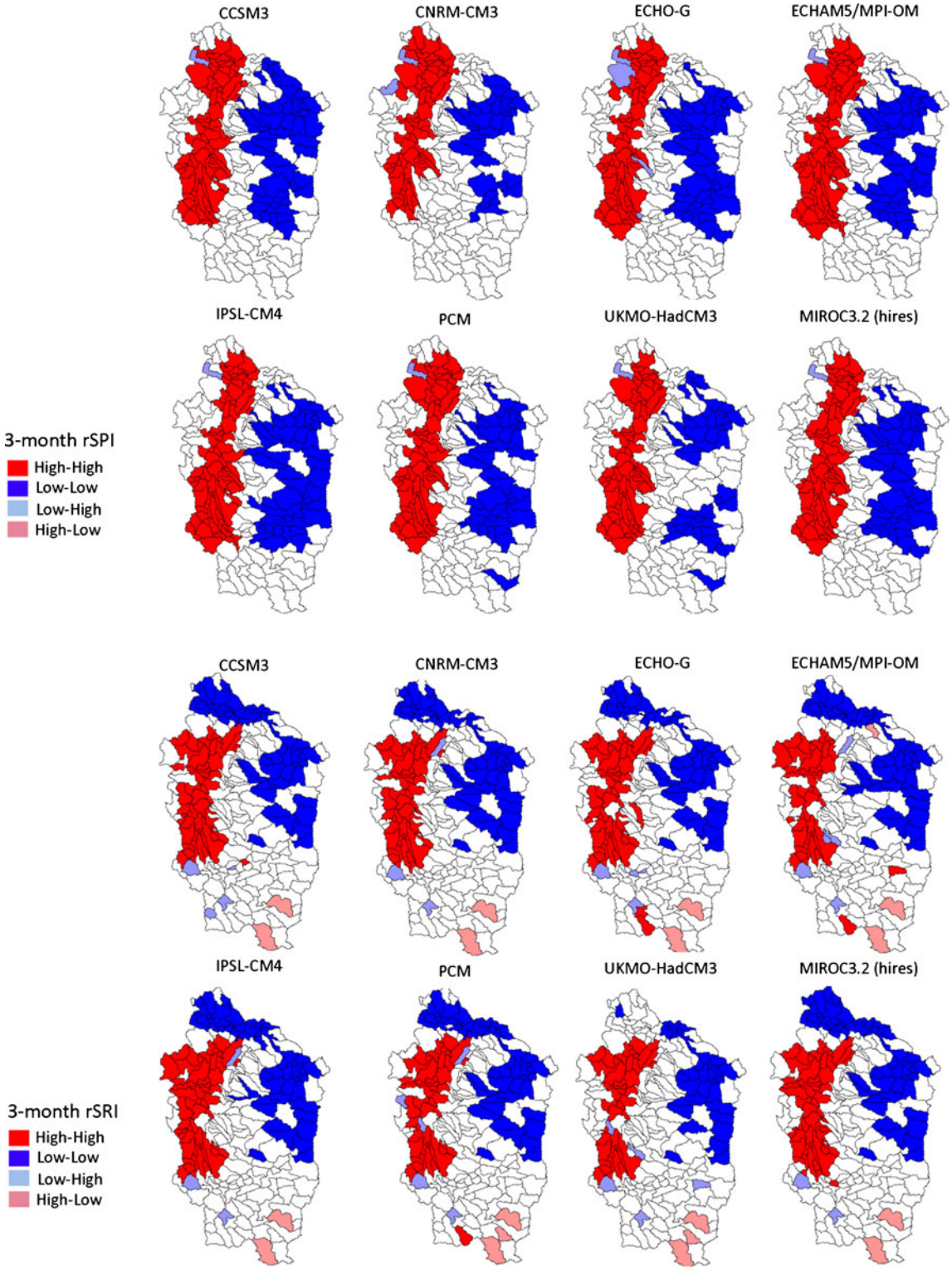

Fig. 11 Results of LISA for 3-month rSPI (*upper two panels*) and rSRI (*lower two panels*) according to eight GCMs with B1 GHG emission scenario. High–High is hot spot and Low–Low is cold spot. This analysis is based on the result of the 2080s period

examined whether their spatial changes are consistent according to different GCMs, GHG emission scenarios, or drought indices using LISA. Figure 10 shows hot spots and cold spots of drought frequency change under the A1B scenario, while Fig. 11 shows hot and cold spots under the B1 scenario. One interesting result is that the location and extent of hot and cold spots generally remain consistent among different GCMs and GHG emission scenarios. Hot

spots indicate that neighboring watersheds are expected to have high changes in drought frequency and cold spots represent a cluster of corresponding low changes in drought frequency. Therefore, this result shows that watersheds in the Willamette Valley could be more affected by climate change than watersheds in the Western and High Cascades. This may be because that the watersheds in the Western and High Cascades could remain more water-rich than the Willamette Valley. As shown in Figs. 10 and 11, the pattern of hot spots slightly varies depending on the drought index used, especially in the Tualatin River in the northwest of the WRB. This result indicates that selection of drought indices would be one of the main sources of uncertainty in spatial patterns of drought risk under climate change in the WRB.

5 Discussion and conclusions

This study aims to identify which WRB regions are vulnerable to possible drought risk of based on statistically downscaled multiple climate simulations with A1B and B1 GHG emission scenarios. Our results show that the Willamette valley region has relatively high drought vulnerability (hot spots), but the High Cascades region has low drought risk (cold spot) because of high summer streamflow and less seasonality due partially to its deep groundwater system. According to the results of LISA, the spatial patterns of drought frequency change could be affected by the choice of drought index. This indicates that the correct drought index would be essential for accurate drought risk analysis. To date, the majority of drought indices have been evaluated for various watersheds (e.g., Shukla and Wood 2008; Vidal et al. 2010; Balling and Goodrich 2010). However, a single drought index is often inadequate for completely representing complex drought phenomenon (Sun et al. 2011). Some studies suggest applying multiple drought indices or integration of drought indices (Steinemann and Cavalcanti 2006; Sun et al. 2011). Because there is no complete drought estimation technique, researchers should employ appropriate drought indices that can represent regional hydro-climatic regimes as well as socioeconomic conditions. This could reduce uncertainty in future drought impact analysis.

This study shows short-term drought risk in the WRB is projected to increase under climate change. This is because of shifts in the timing of flow and reduced summer precipitation based on GCMs simulations. Short-term droughts during the growing season have major implications for agricultural productivity. Recent growing season droughts in 2002 resulted in an estimated net loss of $27 million to $46 million in crop revenues. Also, severe droughts hit eastern Oregon regions in 2005 and 2007, and some reservoirs ran dry months before the end of the growing season (Oregonian 2009). To cope with the threat of such events, we have to prepare robust long-term spatially explicit adaptation strategies and specific actions based on our current knowledge. One solution is improving the water transfer system between water-rich regions and water-poor regions. Our results show that the Western Cascades and the High Cascades will remain as relatively water-rich regions compared to the Willamette Valley even though their hydrology will be significantly affected by climate change. Additionally, improving drought preparedness, increasing the water storage capacity of existing dams and reservoirs, developing new reservoir operation rules, diversifying water resources sources, and enhancing irrigation technologies and water use efficiency could contribute in adapting to climate change.

Acknowledgments This research was supported by the Institute for Sustainable Solutions (ISS) at Portland State University. Additional support was provided by US National Science Foundation under grant no. CR-1038925. Any opinions, findings, and conclusions or recommendations expressed in this material are those of the authors and do not necessarily reflect the views of the National Science Foundation. We thank Madeline Steele of Portland State University for proofreading the manuscript and for the helpful comments.

References

Anselin L (1995) Local indicators of spatial autocorrelation—LISA. Geogr Anal 27:93–115

Anselin L, Syabri I, Kho Y (2006) GeoDa: an introduction to spatial data analysis. Geogr Anal 38(1):5–22

Balling RC, Goodrich GB (2010) Increasing drought in the American Southwest? A continental perspective using a spatial analytical evaluation of recent trends. Phys Geogr 31:293–306

Bates BC, Kundzewicz ZW, Wu S, Palutikof JP (Eds) (2008) Climate Change and Water. Technical Paper of the Intergovernmental Panel on Climate Change. IPCC Secretatiat, Geneva, p. 210

Bond NR, Lake PS, Arthington AH (2008) The impacts of drought on freshwater ecosystems: an Australian perspective. Hydrobiologia 600:3–16

Chang HJ, Jung IW (2010) Spatial and temporal changes in runoff caused by climate change in a complex large river basin in Oregon. J Hydrol 388:186–207

Chen ST, Kuo CC, Yu PS (2009) Historical trends and variability of meteorological droughts in Taiwan. Hydrol Sci J-J Des Sci Hydrol 54:430–441

Daly C, Neilson RP, Phillips DL (1994) A statistical topographic model for mapping climatological precipitation over mountainous terrain. J Appl Meteorol 33:140–158

Dezman LE, Shafer BA, Simpson HD, Danielson JA (1982) Development of a surface water supply index—a drought severity indicator for Colorado. Int. Symp. Hydrometeorology, Proc., American Water Resources Association (AWRA), Bethesda, Md., pp. 337–341

Dubrovsky M, Svoboda MD, Trnka M, Hayes MJ, Wilhite DA, Zalud Z, Hlavinka P (2009) Application of relative drought indices in assessing climate-change impacts on drought conditions in Czechia. Theor Appl Climatol 96:155–171

Dubrovsky M, Nemesova I, Kalvova J (2005) Uncertainties in climate change scenarios for the Czech Republic. Clim Res 29:139–156

Franczyk J, Chang H (2009a) Spatial analysis of water use in Oregon, USA, 1985–2005. Water Resour Manag 23:755–774

Franczyk J, Chang H (2009b) The effects of climate change and urbanization on the runoff of the Rock Creek basin in the Portland metropolitan area, Oregon, USA. Hydrol Process 23:805–815

Gebrehiwot T, van der Veen A, Maathuis B (2011) Spatial and temporal assessment of drought in the Northern highlands of Ethiopia. Int J Appl Earth Obs Geoinformation 13:309–321

Greenough G, McGeehin M, Bernard SM, Trtanj J, Riad J, Engelberg D (2001) The potential impacts of climate variability and change on health impacts of extreme weather events in the United States. Environ Heal Perspect 109:191–198

Guttman NB (1999) Accepting the standardized precipitation index: a calculation algorithm. J American Water Resour Assoc 35:311–322

Hamlet AF, Lettenmaier DP (2005) Production of temporally consistent gridded precipitation and temperature fields for the continental United States. J Hydrometeorol 6:330–336

Heim RR (2002) A review of twentieth-century drought indices used in the United States. Bull Am Meteorol Soc 83:1149–1165

Huntington TG (2006) Evidence for intensification of the global water cycle: review and synthesis. J Hydrol 319:83–95

IPCC (2007) Climate Change 2007: The Physical Science Basis. Contribution of Working Group I to the Fourth Assessment Report of the Intergovernmental Panel on Climate Change [Solomon, S., D. Qin, M. Manning, Z. Chen, M. Marquis, K.B. Averyt, M.Tignor and H.L. Miller (eds.)]. Cambridge University Press, Cambridge, United Kingdom and New York, NY, USA

Jung IW, Chang HJ (2011) Assessment of future runoff trends under multiple climate change scenarios in the Willamette River Basin, Oregon, USA. Hydrol Process 25:258–277

Jung IW, Chang H, Moradkhani H (2011) Quantifying uncertainty in urban flooding analysis considering hydro-climatic projection and urban development effects. Hydrol Earth Syst Sci 15:617–633

Kangas RS, Brown TJ (2007) Characteristics of US drought and pluvials from a high-resolution spatial dataset. Int J Climatol 27:1303–1325

Kasei R, Diekkruger B, Leemhuis C (2010) Drought frequency in the Volta Basin of West Africa. Sustain Sci 5:89–97

Kogan FN (1995) Droughts of the late 1980s in the United States as derived from NOAA polar-orbiting satellite data. Bull Am Meteorol Soc 76(5):655–668

Krause P, Boyle DP, Bäse F (2005) Comparison of different efficiency criteria for hydrological model assessment. Adv Geosci 5:89–97

Krysanova V, Vetter T, Hattermann F (2008) Detection of change in drought frequency in the Elbe basin: comparison of three methods. Hydrol Sci J-J Des Sci Hydrol 53:519–537

Laenen A, Risley JC (1997) Precipitation-runoff and streamflow-routing models for the Willamette River Basin, Oregon. US Geological Survey Water Resources Investigations Report 95–4284

Lorenzo-Lacruz J, Vicente-Serrano SM, Lopez-Moreno JI, Begueria S, Garcia-Ruiz JM, Cuadrat JM (2010) The impact of droughts and water management on various hydrological systems in the headwaters of the Tagus River (central Spain). J Hydrol 386:13–26

McFarland WD (1983) A description of aquifer units in Western Oregon: US Geological Survey Open-File Report 82–165, 35 p

McKee TB, Doesken NJ, Kleist J (1993) Drought monitoring with multiple timescales. Preprints, Eighth Conf. on Applied Climatology, Anaheim, CA, Am Meteor. Soc., pp. 179–184

Mishra AK, Singh VP (2009) Analysis of drought severity-area-frequency curves using a general circulation model and scenario uncertainty. Journal of Geophysical Research-Atmospheres 114

Mote P, Salathe E (2010) Future climate in the Pacific Northwest. Climate Change 102:29–50

Natural Resources Conversation Service (NRCS) (1986) General soil map, state of Oregon: Portland, Oregon, Natural Resource Conservation Service, scale 1:1000,000

Oregonian (2009) New study shows river runoff decreases in driest years in Oregon, Northwest. http://www.oregonlive.com/news/index.ssf/2009/09/new_study_shows_oregon.html. (accessed 07.19.11)

Palmer WC (1965) Meteorological drought. Weather Bureau, Research Paper No. 45. U.S. Dept. of Commerce, Washington, p 58

Palmer WC (1968) Keeping track of crop moisture conditions, nationwide: the new crop moisture index. Weatherwise 21:156–161

Parzen E (1962) On estimation of a probability density function and mode. Annals of Mathematical Statistics 33:1065–1076

Phillips ID, McGregor GR (1998) The utility of a drought index for assessing the drought hazard in Devon and Cornwall, South West England. Meteorol Appl 5:359–372

Quiring SM, Ganesh S (2010) Evaluating the utility of the Vegetation Condition Index (VCI) for monitoring meteorological drought in Texas. Agric For Meteorol 150:330–339

Randall DA, Wood RA, Bony S, Colman R, Fichefet T, Fyfe J, Kattsov V, Pitman A, Shukla J, Srinivasan J, Stouffer RJ, Sumi A, Taylor KE (2007) Climate models and their evaluation. In: Solomon S, Qin D, Manning M, Chen Z, Marquis M, Averyt KB, Tignor M, Miller HL (Eds.), Climate Change 2007: The Physical Science Basis. Contribution of Working Group I to the Fourth Assessment Report of the Intergovernmental Panel on Climate Change. Cambridge University Press, Cambridge, United Kingdom and New York, NY, USA, 589–662

Risley J, Moradkhani H, Hay L, Markstrom S (2011) Statistical comparisons of watershed-scale response to climate change in selected basins across the United States. Earth Interact 15:26

Salathe EP, Mote PW, Wiley MW (2007) Review of scenario selection and downscaling methods for the assessment of climate change impacts on hydrology in the United States Pacific Northwest. Int J Climatol 27:1611–1621

Shukla S, Wood AW (2008) Use of a standardized runoff index for characterizing hydrologic drought. Geophysical Research Letters 35

Steinemann AC, Cavalcanti LFN (2006) Developing multiple indicators and triggers for drought plans. J Water Resour Plan Manag 132 (3):164–174

Strzepek K, Yohe G, Neumann J, Boehlert B (2010) Characterizing changes in drought risk for United States from climate change. Environ Res Lett 5(044012). doi:10.1088/1748-9326/5/4/044012

Sun L, Mitchell SW, Davidson A (2011) Multiple drought indices for agricultural drought risk assessment on the Canadian prairies. Int J Climatol. doi:10.1002/joc.2385

Tague C, Grant G, Farrell M, Choate J, Jefferson A (2008) Deep groundwater mediates streamflow response to climate warming in the Oregon Cascades. Climate Change 86:189–210

Ummenhofer CC, England MH, McIntosh PC, Meyers GA, Pook MJ, Risbey JS, Gupta AS, Taschetto AS (2009) What causes southeast Australia's worst droughts? Geophysical Research Letters 36: L04706

US Geological Survey (USGS) Seamless (2011) National Map Seamless Server. <http://seamless.usgs.gov/index.php> (accessed 07.19.11)

US Geological Survey National Water Information System (USGS NWIS) (2011) USGS Surface-Water Statistics for Oregon. http://waterdata.usgs.gov/or/nwis/ (accessed 07.19.11)

Vergni L, Todisco F (2011) Spatio-temporal variability of precipitation, temperature and agricultural drought indices in Central Italy. Agric For Meteorol 151:301–313

Vicente-Serrano SM, Beguería S (2003) Estimating extreme dry-spell risk in the middle Ebro valley (Northeastern Spain): a comparative analysis of partial duration series with a General Pareto

distribution and annual maxima series with a Gumbel distribution. Int J Climatol 23:1103–1118

Vidal JP, Wade S (2009) A multimodel assessment of future climatological droughts in the United Kingdom. Int J Climatol 29:2056–2071

Vidal JP, Martin E, Franchisteguy L, Habets F, Soubeyroux JM, Blanchard M, Baillon M (2010) Multilevel and multiscale drought reanalysis over France with the Safran-Isba-Modcou hydrometeorological suite. Hydrol Earth Syst Sci 14:459–478

Willmott CJ (1982) Some comments on the evaluation of model performance. Bull Am Meteorol Soc 63:1309–1313

Wood AW, Leung LR, Sridhar V, Lettenmaier DP (2004) Hydrologic implications of dynamical and statistical approaches to downscaling climate model outputs. Climate Change 62:189–216